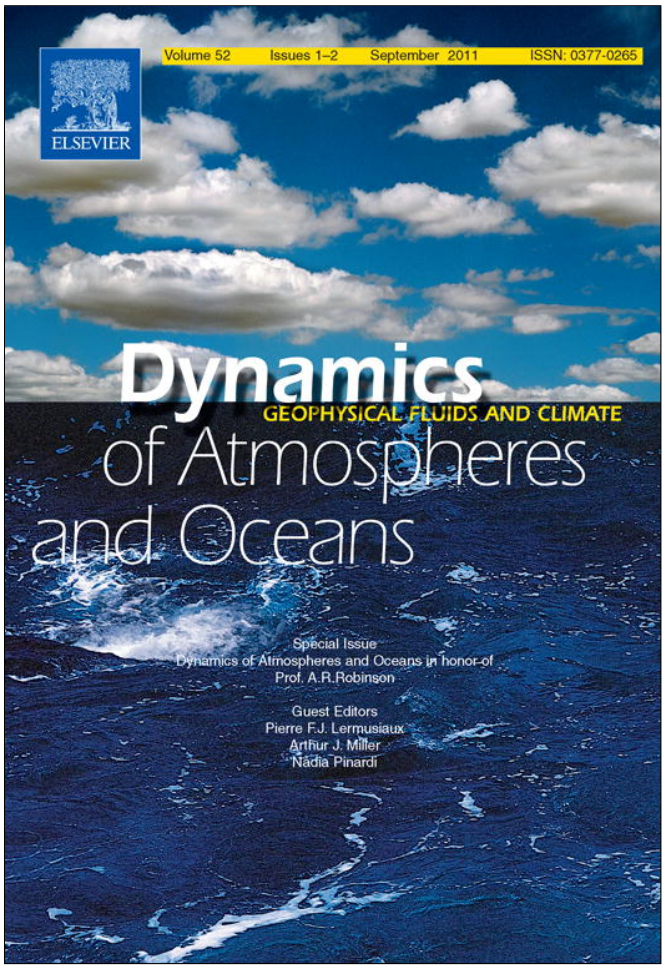

Dynamics of Atmospheres and Oceans 52 (2011) 80–94

Contents lists available at ScienceDirect

Dynamics of Atmospheres and Oceans

journal homepage: www.elsevier.com/locate/dynatmoce

Impact of eddy–wind interaction on eddy demographics and phytoplankton community structure in a model of the North Atlantic Ocean

Laurence A. Anderson[a,*], Dennis J. McGillicuddy Jr.[a], Mathew E. Maltrud[b], Ivan D. Lima[c], Scott C. Doney[c]

[a] Department of Applied Ocean Physics and Engineering, Woods Hole Oceanographic Institution, Woods Hole, MA, USA
[b] Fluid Dynamics Group, Theoretical Division, Los Alamos National Laboratory, Los Alamos, NM, USA
[c] Department of Marine Chemistry and Geochemistry, Woods Hole Oceanographic Institution, Woods Hole, MA, USA

ARTICLE INFO

Available online 26 January 2011

Keywords:
Mesoscale eddies
Phytoplankton
Community composition
Air–sea interaction
Wind stress
Ekman pumping
25–30°N 58–68°W

ABSTRACT

Two eddy-resolving (0.1°) physical–biological simulations of the North Atlantic Ocean are compared, one with the surface momentum flux computed only from wind velocities and the other using the difference between air and ocean velocity vectors. This difference in forcing has a significant impact on the intensities and relative number of different types of mesoscale eddies in the Sargasso Sea. Eddy/wind interaction significantly reduces eddy intensities and increases the number of mode-water eddies and "thinnies" relative to regular cyclones and anticyclones; it also modifies upward isopycnal displacements at the base of the euphotic zone, increasing them in the centers of mode water eddies and at the edges of cyclones, and decreasing them in the centers of cyclones. These physical changes increase phytoplankton growth rates and biomass in mode-water eddies, bringing the biological simulation into better agreement with field data. These results indicate the importance of including the eddy/wind interaction in simulations of the physics and biology of eddies in the subtropical North Atlantic. However, eddy intensities in the simulation with eddy/wind interaction are lower than observed, which suggests a decrease in horizontal viscosity or an increase in horizontal grid resolution will be necessary to regain the observed level of eddy activity.

* Corresponding author at: Bigelow Bldg, Rm 411, WHOI–MS #9, Woods Hole, MA 02543, USA. Tel.: +1 508 289 3742; fax: +1 508 457 2194.
E-mail address: landerson@whoi.edu (L.A. Anderson).

0377-0265/$ – see front matter © 2011 Elsevier B.V. All rights reserved.
doi:10.1016/j.dynatmoce.2011.01.003

1. Introduction

Recent field observations in the Sargasso Sea exhibit relationships between different phytoplankton groups and different types of mesoscale eddies. Enhanced diatom and dinoflagellate biomass has been found in mode-water eddies (Sweeney et al., 2003; McGillicuddy et al., 2007; Benitez-Nelson and McGillicuddy, 2008; Mouriño-Carballido, 2009; Krause et al., 2010). Enhanced *Prochlorococcus* and *Synechococcus* biomass has been observed in cyclones (Sweeney et al., 2003; Mouriño-Carballido, 2009). Enhanced biomass of nitrogen-fixing *Trichodesmium* spp. has been found associated with anticyclones (Davis and McGillicuddy, 2006). Unfortunately in most cases the data are insufficient to determine whether these relationships are due to in situ growth, horizontal advection across large-scale gradients, or local aggregation.

Intensive field observations in the Sargasso Sea in 2005 found persistent upwelling at 100 m depth at the core of an anticyclonic mode-water eddy (Ledwell et al., 2008). This was attributed to a surface divergence caused by variations in wind stress across the eddy. The air-to-sea momentum flux is smaller on the side of an eddy where wind and currents are in the same direction, compared to the other side where wind and currents are in opposite directions. This generates a divergence in the horizontal Ekman transport at the center of an anticyclone (and convergence in a cyclone) regardless of wind direction, driving vertical velocities at the base of the Ekman layer which can penetrate to the main thermocline at the center of eddies (Dewar and Flierl, 1987; Martin and Richards, 2001). For brevity this will be referred to as "eddy/wind interaction". Eddy/wind interaction was apparently the driver behind the increased diatom biomass and primary productivity found within the eddy (McGillicuddy et al., 2007).

Until recently, most eddy-resolving models have used surface momentum fluxes computed from wind velocities alone, and thus do not include the impact of eddy/wind interaction on vertical velocities and eddy characteristics. Recent simulations show that including eddy/wind interaction significantly decreased the amount of energy in the mesoscale eddy field (Zhai and Greatbatch, 2007; Xu and Scott, 2008; Small et al., 2009). Eden and Dietze (2009) found that including the eddy/wind interaction caused a 10–50% reduction in eddy activity though only a 5% reduction in new production.

Here we compare the results of two eddy-resolving physical–biological simulations of the North Atlantic Ocean, one of which computes the surface momentum flux only from wind velocity vectors, and the other using air-minus-ocean velocity vectors. First we describe differences in the mean physical structure of mesoscale eddies in the two cases. We then examine how these physical differences impact the relationships between eddy type and simulated phytoplankton species composition. We concentrate on the Sargasso Sea, where data for comparison are relatively abundant. However, even in this relatively data-rich area, the number of synoptic realizations of mesoscale biological and biogeochemical distributions is insufficient to deduce reliable statistics that can be compared directly with the model. We therefore focus our model-data comparisons on qualitative aspects, such as whether or not the model is able to simulate the distinct biological responses to each of the various types of eddies.

2. Methods

The coupled physical–biogeochemical model is based on the Los Alamos Parallel Ocean Program (Smith et al., 1992, 2000). It was configured for the North Atlantic (20°S–72°N) using an "eddy-resolving" horizontal grid resolution of $11.1 \cos\phi$ km, where ϕ is latitude. The primary differences between these runs using POP 2.0.1 and the POP 1.1.1 simulations described in McGillicuddy et al. (2003) are as follows. The number of time steps per day was increased from 150 to 200 for sufficient numerical precision of the biological model. The number of vertical levels was increased from 40 to 42 (viz. the maximum depth increased from 5500 m to 6000 m). Partial bottom cells were included to better simulate the interaction of currents with bathymetry. Vertical mixing was switched from explicit-in-time with convective adjustment to implicit-in-time, and from Richardson number dependent (Pacanowski and Philander, 1981) to KPP (Large et al., 1994). Horizontal viscosity was changed from biharmonic only ($-27e{+}9\ m^4\ s^{-1}$) to biharmonic plus Laplacian ($-6.75e{+}9\ m^4\ s^{-1}$ and $35.5\ m^2\ s^{-1}$; Hecht et al., 2008). The air–sea drag coefficient was changed from wind-speed dependent

only (Large and Pond, 1981) to air–sea stability dependent (Large and Pond, 1982). The heat forcing was changed from a shortwave flux plus restoring to monthly SST climatology (Barnier et al., 1995) to heat fluxes computed from bulk formulae using NCEP atmospheric variables (air temperature, humidity, wind speed, shortwave and downward longwave flux) and model SST. Surface salinity forcing was changed from restoring to monthly salinity climatology to monthly precipitation climatology plus evaporation based on the latent heat flux. The model forcing was changed to a 6-h, repeating "normal-year" atmospheric forcing (Large and Yeager, 2004), so that the interannual variability in the circulation would be due solely to dynamic adjustment and not due to interannual variability in the forcing.

A 24-box biogeochemical–ecosystem model (BEC; Moore and Doney, 2007; Moore et al., 2004, 2006) was incorporated into the physical model. This model includes three phytoplankton groups: diatoms (DIAT), small phytoplankton (SP) and N_2-fixing diazotrophs (DIAZ, representing *Trichodesmium* spp.). As such, it can be tested directly with the observed relationships between eddies and phytoplankton species composition mentioned in Section 1. The limiting nutrients are PO_4, NO_3, NH_4, Fe and SiO_3 (for diatoms). The MPDCD advection scheme was used for biological tracers (Oschlies and Garcon, 1999), which is a centered-difference advection scheme with a flux limiter to prevent negative tracer values.

BEC model parameters were mostly the same as in Moore and Doney (2007), although several parameters were tuned to improve agreement with observations in the North Atlantic. This was accomplished by simultaneously optimizing with data (NO_3, PO_4, Chl, HPLC-estimated diatom Chl, primary production and sinking POC flux) from the Bermuda Atlantic Time Series (BATS; Steinberg et al., 2001) at 32°N 64°W and North Atlantic Bloom Experiment (NABE; Ducklow and Harris, 1993) at 47°N 20°W using the Regional Testbed model (Friedrichs et al., 2007). The biological model parameter changes included the following: reducing the diatom mortality threshold (*loss_thres_diat* from 0.01 to 0.001 μM C) to lower diatom biomass in the subtropical gyre but not in high latitudes; increasing the small phytoplankton and diatom PO_4 uptake half-saturation coefficients (*sp_kPO4* from 0.0003125 to 0.005 μM, *diat_kPO4* from 0.005 to 0.02 μM) both to increase surface PO_4 toward observed values, which consequently improved the diazotroph vertical distribution; and increasing the diatom and small phytoplankton maximum growth rate at 30 °C (*PCref* from 3.0 to 3.6 d^{-1}) and increasing the zooplankton grazing half-saturation constant (*z_grz* from 1.05 to 1.35 μM C), which increase total Chl and primary production.

The coupled physical–biological simulation was initialized with World Ocean Atlas 2001 January temperature, salinity and nutrients (Stephens et al., 2002; Boyer et al., 2002; Locarnini et al., 2002; Conkright et al., 2002), GLODAP climatology dissolved inorganic carbon and alkalinity (Key et al., 2004) and the other biological state variables with year 800 results of a coarse-resolution global simulation. This simulation was run for 14.5 years until quasi-equilibrium. The changes to the biological model parameter values mentioned in the preceding paragraph were then made, the nutrients (NO_3, PO_4, SiO_3 and O_2) re-initialized with World Ocean Atlas 2005 July distributions (Garcia et al., 2006a,b), and the coupled model run for 7 more years. Basin-averaged kinetic energy shows short-term temporal variability, but appears to be in quasi-equilibrium in the last 7 years of simulation (Fig. 1a of the online Supplementary Material). The biological fields reached quasi-equilibrium after approximately 3 years of spin-up (Supplementary Fig. 1b), in part due to the fact that semi-labile dissolved organic carbon, nitrogen and phosphorus were not starting from constant values but from near-equilibrium large-scale distributions.

Model output was saved as 5-day averages. Large-scale spatial trends were computed from each 5-day average by spatially smoothing with a Gaussian filter with a 3° (30 grid point) e-folding scale and a 7.5° maximum radius. The difference between each 5-day average and its large-scale spatial trend was used to estimate the mesoscale anomaly field. Although the model solution clearly contains submesoscale variability, it is underrepresented at this grid resolution (Lévy et al., 2001). For eddy locating purposes only, further smoothing of sea level anomaly and density with a 0.4° e-folding scale Gaussian filter (maximum radius 1.0°) was used to filter out submesoscale structure. To be approximately consistent with the location of the BATS data and EDDIES field observations, model output is examined in a Sargasso subdomain between 25–30°N and 58–68°W for year days 150–275 of the last 4 years of the simulation. The observations extend to 32°N, but the domain is shifted 2° south to avoid the strong influence of Gulf Stream rings on the analysis.

3. Results

The simulation that uses the surface momentum flux computed only from wind velocities will be referred to as "Run 1" (no eddy/wind interaction), and the simulation that uses the difference between air and ocean velocities will be referred to as "Run 2" (with eddy/wind interaction).

Eddies were identified as extrema in mesoscale sea level anomaly (SLA), and classified as one of four types: regular cyclone ("C"; negative SLA and positive density anomaly at 97 m), regular anticyclone ("A"; positive SLA and negative density anomaly at 97 m), mode-water eddy ("M"; positive SLA and positive density anomaly) and "thinny" ("T"; negative SLA and negative density anomaly). The name "thinny" derives from the fact that in the Sargasso these eddies have a relatively "thin" layer of 18° mode water between 100 m and the main thermocline at 700 m, while "mode-water" eddies have a relatively thick layer. In both cases, displacement of the main thermocline dominates geostrophic velocities and SLAs, such that thinnies are cyclonic and mode-water eddies are anticyclonic. The density anomaly at 97 m is of particular interest because in the Sargasso it is the approximate depth of the nitracline, the deep chlorophyll maximum, and the base of the euphotic zone. Isopycnal displacements at this depth are thus expected to induce a biological response (McGillicuddy et al., 1999). This classification method can be misleading when and where mixed-layer depth exceeds 97 m (i.e. in winter), and thus we restrict our period of analysis accordingly.

Mean vertical transects of various properties through each type of eddy for Run 2 (with eddy–wind interaction) are given in online Supplementary Figs. 2–7. As the eddy-induced horizontal gradients in all properties of interest are small compared with vertical gradients, background profiles were removed to reveal the anomaly fields, which indicate the modulation the eddies cause to the mean. These anomaly transects (also given in online Supplementary Figs. 2–7) show different responses in the euphotic zone and the aphotic zone, typically divided at 104 m (which is the bottom interface of the model grid box centered at 97 m). Consequently 0–104 m vertical integrals and fluxes at 104 m are presented below. These summarize the euphotic zone results, where mesoscale biological responses are most pronounced. In the simulations, small phytoplankton and diatoms have little biomass below 104 m, such that deeper vertical integrals of their biomass or primary production are very similar.

Standard errors presented below were computed by dividing the standard deviations (computed from 100 five-day averages) by the square root of the number of "independent observations". For this we use the number of independent eddies as determined by eddy tracking, which for Run 1 is 45 C, 40 A, 32 M and 19 T, and for Run 2 is 32 C, 29 A, 36 M and 28 T. Naturally, this approximately equals the total number of eddies of each type counted in all 100 frames divided by the mean temporal correlation timescale, which is approximately one month (6 frames). We also include in the standard errors the uncertainty related to removing the large-scale spatial trend. This was done by varying the spatial scales in the computation of the large-scale trend by ±20% (±33% gave unacceptably poor separation of the large-scale trend from mesoscale anomalies), and estimating this error as the mean difference of these cases from the standard case. The detrending errors and eddy-variance errors were then combined.

3.1. Physical simulation results

As in previous studies (Zhai and Greatbatch, 2007; Xu and Scott, 2008; Small et al., 2009; Eden and Dietze, 2009), the standard deviation of sea level anomaly (SLA) declined from Run 1 to Run 2 (Fig. 1). Comparison of Fig. 1b with the observation-based estimates in Fig. 4a of Scharffenberg and Stammer (2010) shows a significant underestimation of sea level variability throughout the basin except for the Gulf Stream. Nevertheless, both runs exhibit an energetic mesoscale environment, as evidenced by a zoomed-in view of a subdomain in the Sargasso Sea (Fig. 2a and b). The correlation between SLA and negative density anomaly at 729 m is very high, exceeding 0.94 in Run 1. Yet density anomalies at 97 m show a greater amount of submesoscale variance, and often occur at the edges of eddies in both runs (Fig. 2c and d). The mean amplitude of SLA perturbations at the center of all eddy types in the Sargasso Sea drops by about a factor of two from Run 1 to Run 2 (Fig. 3a and b). This is the expected response, as eddy/wind interaction drives downwelling in cyclones and upwelling in anticyclones, and thus is a mechanism that accelerates eddy decay (Dewar and Flierl, 1987).

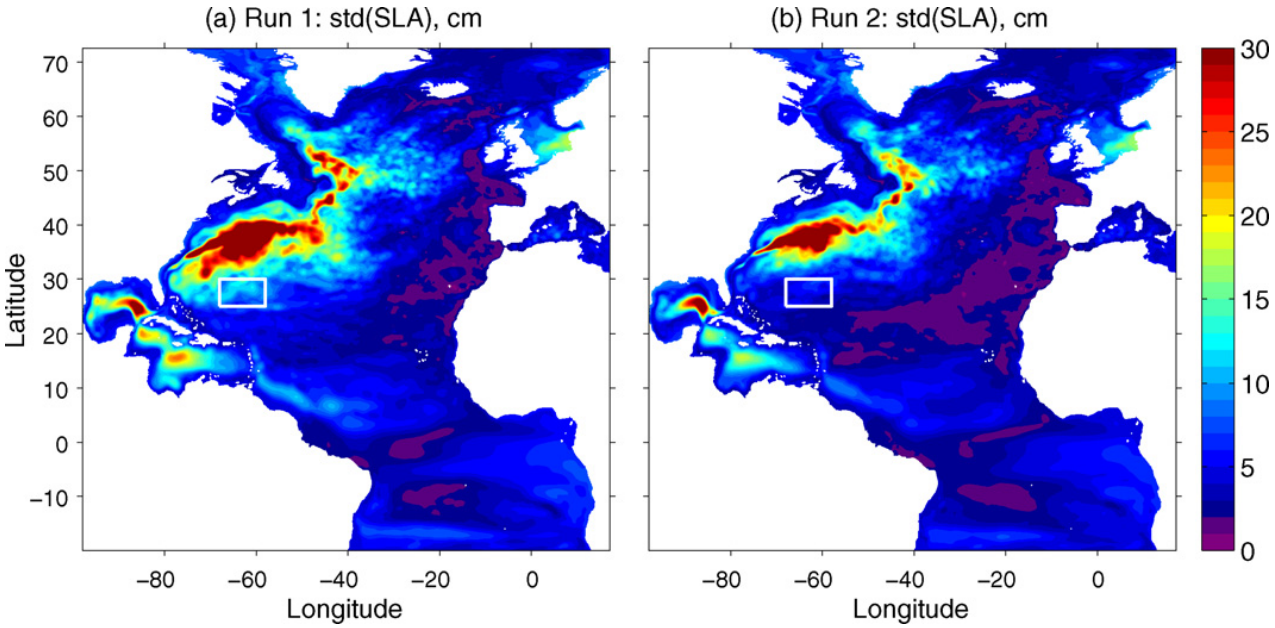

Fig. 1. Standard deviation of sea level anomaly (SLA) in (a) Run 1 (no eddy/wind interaction) and (b) Run 2 (with eddy/wind interaction). The white box is the Sargasso Sea subdomain. In this figure only, SLA is computed as the anomaly from the 4-year temporal mean, to compare directly with Fig. 4a of Scharffenberg and Stammer (2010).

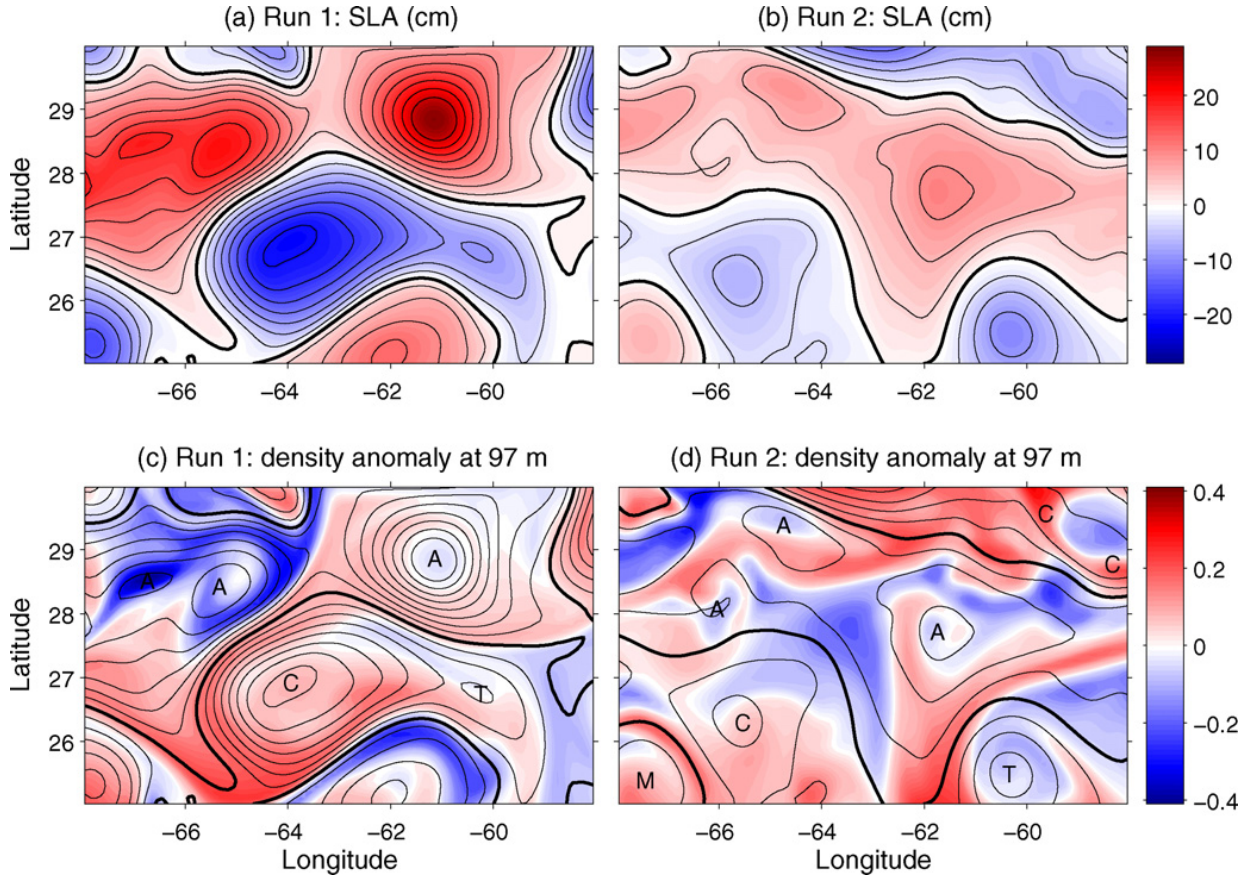

Fig. 2. (a) Run 1 (no eddy/wind interaction) and (b) Run 2 (with eddy/wind interaction) sea level anomaly for the final 5-day average of each run (year 21, days 190–195). SLA is defined as sea surface height with the large-scale spatial trend removed. The thick black line is zero, and the contour interval is 3 cm. (c) Run 1 and (d) Run 2 in situ density anomalies ($kg\,m^{-3}$) at 97 m. SLA contours from (a) and (b) are overlain in black, with eddy types identified based on SLA and density anomaly (C, regular cyclone; A, regular anticyclone; M, mode-water eddy; T, thinny).

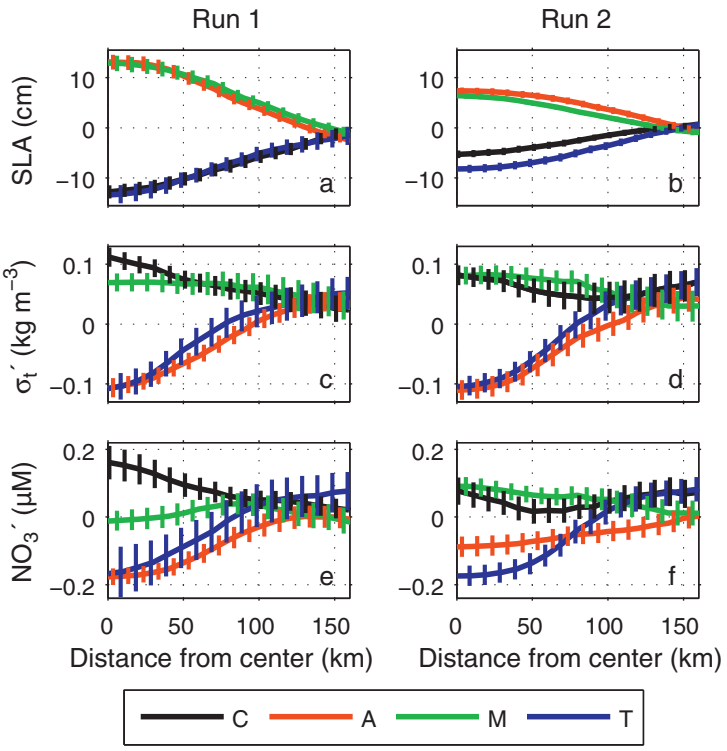

Fig. 3. Mean properties with standard errors of regular cyclones (black), regular anticyclones (red), mode-water eddies (green) and thinnies (blue), as a function of distance from eddy centers, in the Sargasso Sea subdomain for Run 1 (no eddy/wind interaction, left column) and Run 2 (with eddy/wind interaction, right column). The top row shows sea level anomalies. The middle row shows in situ density anomalies at 97 m. The bottom row shows nitrate concentration anomalies at 104 m. From each 5-day average, anomaly fields are computed by removing the large-scale 2D horizontal trends, locating the eddy centers, and aggregating values in the surrounding points into 10-km radial bins. For each of these bins, means and standard deviations are computed. The estimation of standard errors is described in the fourth paragraph of Section 3. (For interpretation of the references to color in this figure legend, the reader is referred to the web version of the article.)

In Run 1 the highest amplitude isopycnal shoaling at 97 m is at the center of cyclones (Fig. 3c), whereas in Run 2 the density anomalies at the center of mode-water eddies and cyclones are comparable. Interestingly in both runs the isopycnals at eddy edges (150 km from eddy center) are on average displaced above the local mean. Examples of this can be seen in Fig. 2c and d where positive density anomalies (red) frequently lie on top of the zero SLA lines. In Run 2, the mean density anomalies at the edges of cyclones and thinnies rival the magnitude of the density anomaly at cyclone centers (Fig. 3d). During the EDDIES experiment, upward displaced isopycnals at eddy edges were sometimes seen (Fig. 3A in Ewart et al., 2008).

Note the error bars in Fig. 3 are standard errors, i.e. the uncertainty in the means, which are roughly 6 times smaller than the standard deviations. By multiplying the error bars in Fig. 3d by a factor of 6, one can see that the variability in radial structure is large, to the point that any individual eddy may not exhibit a clear radial pattern in density at 97 m (Fig. 2d). It is only after averaging over many eddies (400 days in a 5° by 10° domain) that the mean radial patterns emerge.

One would expect eddy/wind interaction to cause upwelling at the center of mode-water eddies and anticyclones and downwelling at the center of cyclones and thinnies. Although the vertical velocities are too variable to distinguish these trends, evidence for their integrated effect is suggested by the nitrate concentration anomalies at 104 m (Fig. 3e and f), which increase from Run 1 to Run 2 at the center of mode-water eddies and anticyclones, and decrease at the center of cyclones, though thinnies change little. These nitrate anomalies at the base of the euphotic zone are modest compared with field observations in mode-water eddies of +0.3 μM at that depth (Table 2 in Li and Hansell, 2008). Also seen is enhanced nitrate at the edges of cyclones and thinnies, similar to and related to the displacements seen in density.

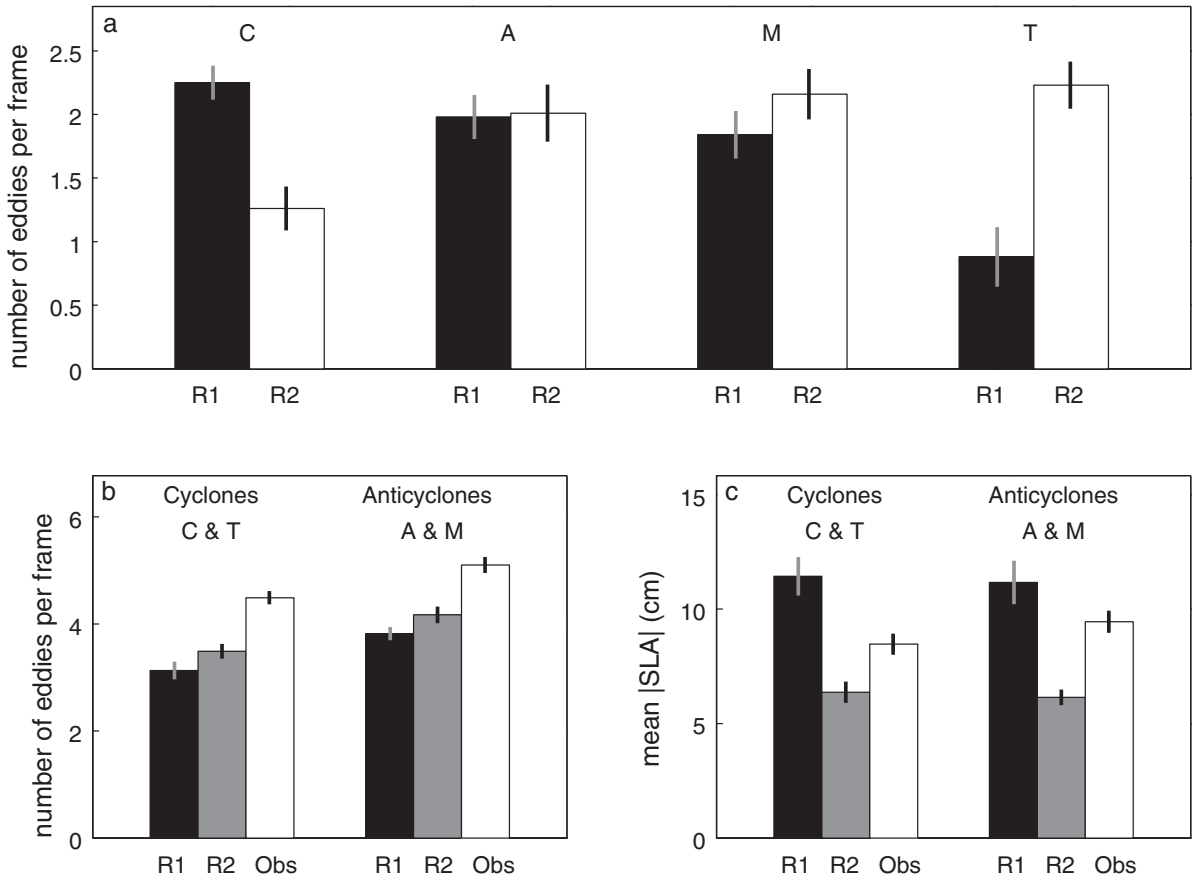

Fig. 4. (a) Mean number of eddies in the Sargasso Sea subdomain (25–30°N, 68–58°W, from 100 frames, viz. 5-day averages from year days 150 to 275 of 4 simulated years) classified based on SLA and density anomaly at 97 m, for Run 1 ("R1", no eddy/wind interaction) and Run 2 ("R2", with eddy/wind interaction). C, regular cyclone; A, regular anticyclone; M, mode-water eddy; T, thinny. The estimation of standard errors is described in the fourth paragraph of Section 3. (b) Mean number of cyclones and anticyclones compared with an observation-based estimate ("Obs") from the 2006–2009 AVISO altimetry data. (c) Mean magnitude of sea level anomaly of cyclones and anticyclones compared with 2006–2009 AVISO altimetry data ("Obs").

The eddy/wind interaction significantly changed the distribution of eddy types (Fig. 4a). The number of regular cyclones decreased and the number of thinnies increased, both by a factor of two. The number of mode-water eddies increased by 17%, though surprisingly the number of regular anticyclones did not change significantly. Observations from the EDDIES cruises provide a means to assess these simulated eddy demographics, although the total number of eddies sampled was relatively small. During EDDIES, 3 of 5 anticyclones investigated turned out to be mode-water eddies, statistically indistinguishable from the 48% and 52% of Run 1 and Run 2. During EDDIES, 1 of 5 cyclones transformed from a cyclone into a thinny during the period of observation, closer to Run 1 (in which 28% of all cyclones are thinnies) than Run 2 (64%). The simulations can also be compared with satellite SLA observations, although the satellite altimetry alone cannot distinguish regular cyclones from thinnies nor regular anticyclones from mode-water eddies, such that comparison can only be made regarding all cyclones (C + T) and all anticyclones (A + M). The AVISO sea level anomaly gridded data were analyzed in the same manner as the model: 5-day averages were retrieved in the Sargasso subdomain between year days 150 and 275 (for years 2006–2009, as before 2006 only 3.5-day analyses are available), and the large-scale spatial trend removed. The number of cyclones and anticyclones in the Sargasso Sea is greater in the observations than in the model, though Run 2 is an improvement over Run 1 (Fig. 4b). SLA amplitude for both cyclones and anticyclones is overestimated in Run 1 (Fig. 4c), while inclusion of eddy–wind interaction decreases SLA amplitudes of both cyclones and anticyclones to below the AVISO estimates. Note the AVISO analysis is performed on a 0.33° longitude grid, and smoothing of the data by objective analysis onto a grid of that resolution may cause underestimation of eddy amplitudes. Thus it is likely the true SLA amplitudes are closer to those of Run 1 than Run 2. Previous

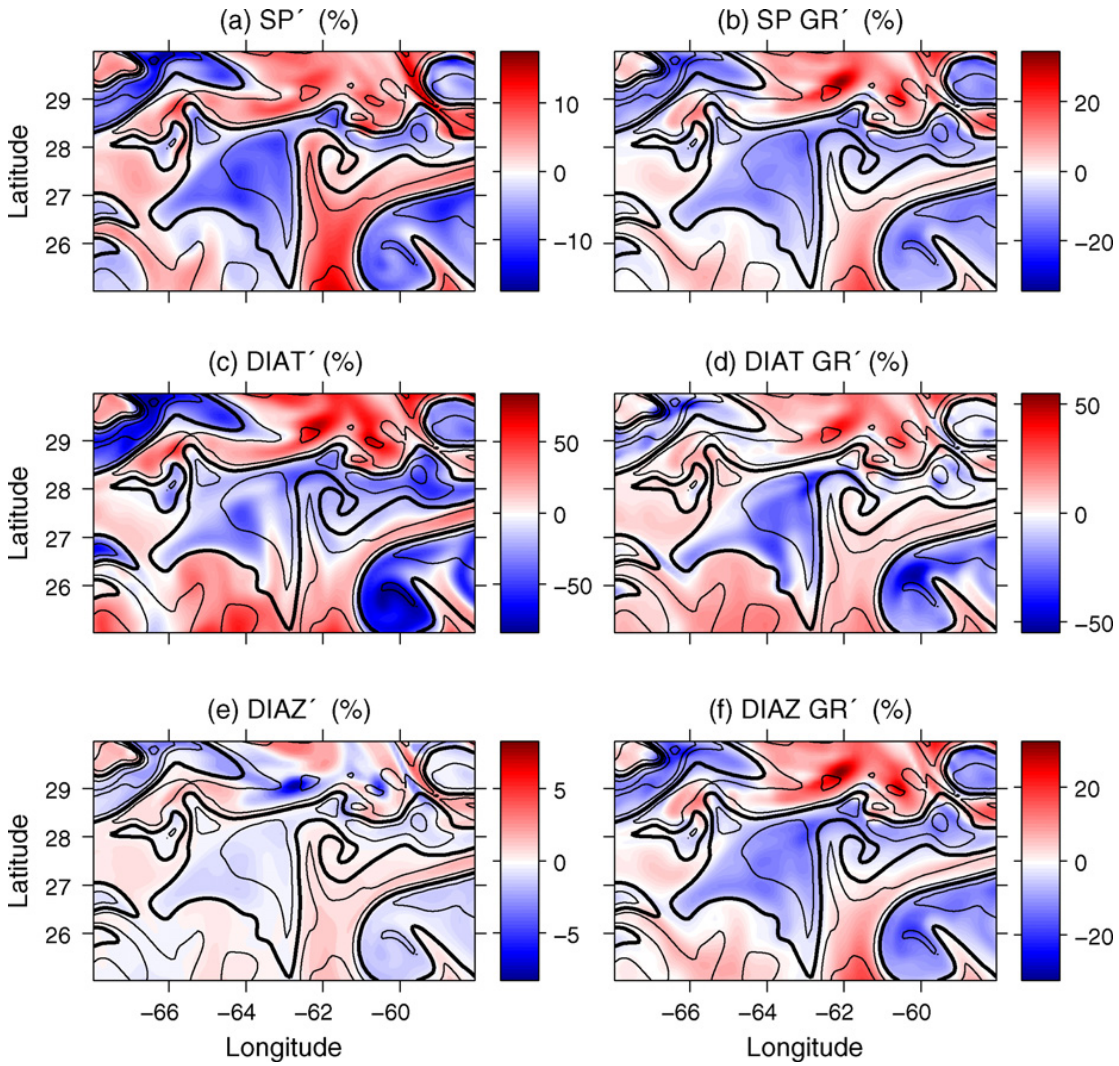

Fig. 5. Run 2 0–104 m vertically integrated phytoplankton biomass (mg C m^{-2}) anomalies, expressed as percent anomaly from large-scale means, for (a) small phytoplankton, (c) diatoms and (e) diazotrophs, for year 21 days 190–195. In situ density anomalies at 97 m (from Fig. 2d) are contoured in black, the thick line being zero, and the contour interval 0.1 kg m^{-3}. Panels (b), (d) and (f) show corresponding specific growth rates (d^{-1}), computed as 0–104 m primary production rates (mg C m^{-2} d^{-1}) divided by 0–104 m biomass (mg C m^{-2}), and expressed as percent anomaly from large-scale mean growth rates, with density anomalies contoured in black. Note that positive biomass and growth rate anomalies for all species correlate with positive density anomalies. Run 1 also shows phytoplankton biomass and growth rate anomalies to be highly correlated with density anomalies. Run 2 is shown because its density anomalies and SLA are less correlated than in Run 1 (Fig. 2), showing the relationship is with density not SLA.

POP 0.1° North Atlantic simulations without eddy/wind interaction have generally shown good agreement with various data types (Smith et al., 2000; McClean et al., 2002; Tokmakian and McClean, 2003; Brachet et al., 2004). Comparison with satellite-based maps of eddy kinetic energy (EKE) (Stammer et al., 2006) also reveals that Run 1 is in better agreement with observations than Run 2.

3.2. Biological simulation results

Spatial structure in the biomass anomalies for all phytoplankton groups tends to correlate positively with density anomalies at 97 m (Fig. 5). As expected, biomass is highest where isopycnal displacements are upward, in response to enhanced specific growth rates, which are due to local uplift of the nitracline and phosphocline (Fig. 3e and f) to higher light intensities.

Phytoplankton biomass and growth rate anomalies show systematic variations as a function of eddy type and distance from eddy center (Figs. 6 and 7). In both runs, biomass and growth rate anomalies

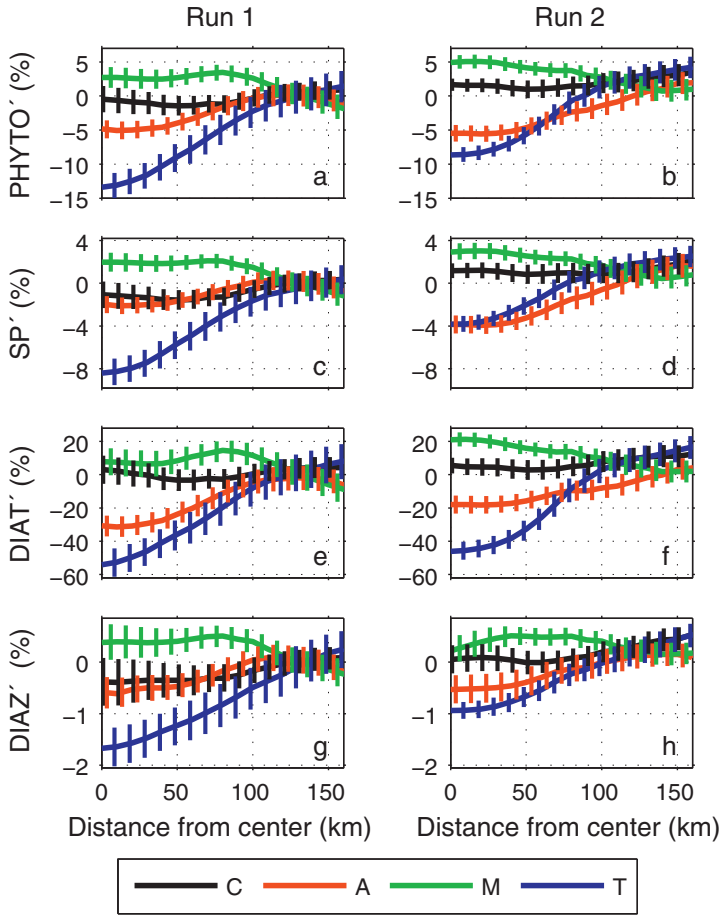

Fig. 6. 0–104 m vertically integrated phytoplankton biomass (mg C m^{-2}) anomalies, expressed as percent anomaly from the large-scale means, with standard errors for regular cyclones (black), regular anticyclones (red), mode-water eddies (green) and thinnies (blue), as a function of distance from eddy centers, in the Sargasso Sea subdomain for Run 1 (no eddy/wind interaction, left column) and Run 2 (with eddy/wind interaction, right column). The top row shows total phytoplankton biomass anomalies; second row, small phytoplankton biomass anomalies; third row, diatom biomass anomalies; bottom row, diazotroph biomass anomalies. From each 5-day average, anomaly fields are computed by removing the large-scale 2D horizontal trends, locating the eddy centers, and aggregating values in the surrounding points into 10-km radial bins. For each of these bins, means and standard deviations are computed. The estimation of standard errors is described in the fourth paragraph of Section 3. (For interpretation of the references to color in this figure legend, the reader is referred to the web version of the article.)

are highest at the center of mode-water eddies, followed by cyclones, then generally anticyclones followed by thinnies. Biomass and growth rate anomalies are also significantly positive at the outer edges of cyclones and thinnies, which has at times been observed (Ewart et al., 2008; Mouriño-Carballido, 2009). Including the eddy/wind interaction significantly increases the diatom growth rate and biomass anomalies at the center of mode-water eddies, increases small phytoplankton and diazotroph anomalies at the center of cyclones from negative to positive, and increases the anomalies at the edges of cyclones and thinnies. The EDDIES cruises did find higher Chl (and in particular diatoms) in mode-water eddies than in cyclones. Thus the eddy/wind interaction brings the simulation into better agreement with observations of mesoscale variations in phytoplankton community composition. Neither run, however, reproduced the observed correlation between diazotrophs and anticyclones (see Section 4).

Another way to visualize the model results which includes all grid points, not just eddies, is to bin properties according to SLA and density anomaly at 97 m, separating the four eddy types into four quadrants (Figs. 8 and 9). The first obvious difference is that the ranges of both SLA and density anomalies in Run 2 are about half those of Run 1. The range and variance of density anomalies at 100 m observed at BATS are actually closer to Run 2 than Run 1 (not shown). Regarding biomass anomalies (Fig. 8), Run 2 shows positive phytoplankton biomass anomalies in mode-water eddies and cyclones, and negative anomalies in anticyclones and thinnies. The relationship is primarily a function of density anomaly rather than SLA. The highest biomass anomalies are for diatoms, which is

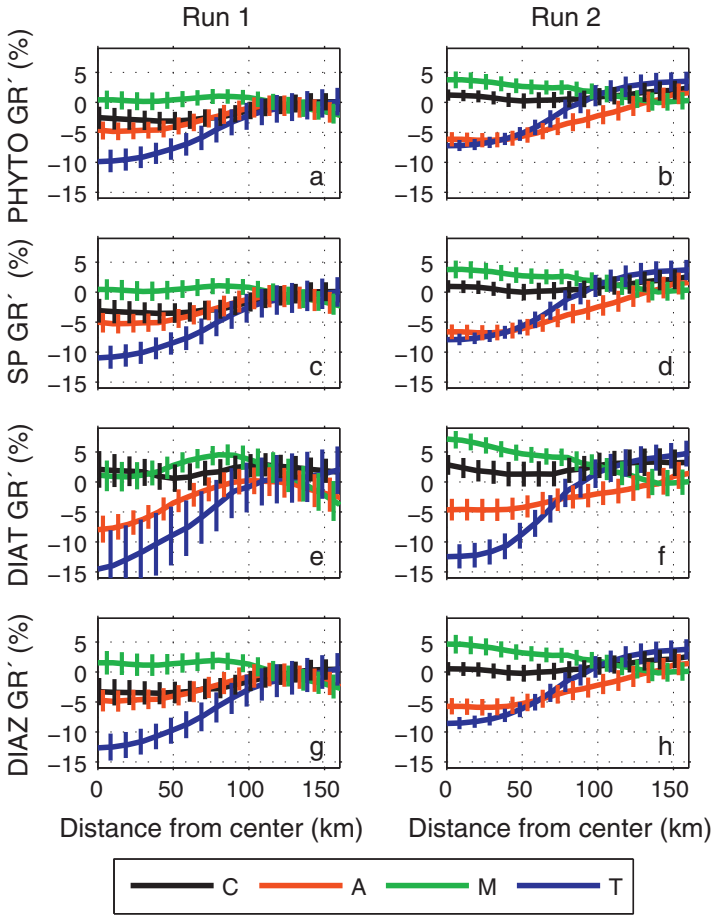

Fig. 7. Specific growth rate anomalies with standard errors for regular cyclones (black), regular anticyclones (red), mode-water eddies (green) and thinnies (blue), as a function of distance from eddy centers, in the Sargasso Sea subdomain for Run 1 (no eddy/wind interaction, left column) and Run 2 (with eddy/wind interaction, right column). The top row shows total phytoplankton growth rate (d^{-1}) anomalies, computed as 0–104 m primary production rates (mg C m^{-2} d^{-1}) divided by 0–104 m biomass (mg C m^{-2}), and expressed as percent anomaly from large-scale mean growth rates. The second row shows small phytoplankton specific growth rate anomalies; third row, diatom specific growth anomalies; bottom row, diazotroph specific growth rate anomalies. From each 5-day average, anomaly fields are computed by removing the large-scale 2D horizontal trends, locating the eddy centers, and aggregating values in the surrounding points into 10-km radial bins. For each of these bins, means and standard deviations are computed. The estimation of standard errors is described in the fourth paragraph of Section 3. (For interpretation of the references to color in this figure legend, the reader is referred to the web version of the article.)

qualitatively consistent with observations; however, the magnitude of the anomalies is still lower than observed (McGillicuddy et al., 2007). The background shading in Fig. 8 shows the general tendency of field data, discussed below (Section 4). Highest growth rate anomalies for all phytoplankton species are found in mode-water eddies and cyclones, up to +28% to +39%, again in response to near-surface isopycnal displacements (Fig. 9) bringing nutrients into higher light intensities.

4. Discussion

Run 2 (with eddy/wind interaction) better represents some basic aspects of observed mesoscale perturbations to phytoplankton species composition. Both Run 2 and observations agree on the strongest biological response being that of diatoms at the center of mode-water eddies, followed by small phytoplankton in mode-water eddies and cyclones. While neither run suggests a significant mean enhancement in diatoms at the center of cyclones (Fig. 6e and f), enhanced diatoms do occur in some cyclones (Fig. 8), often as submesoscale azimuthal variability. This has not been observed in the Sargasso Sea, though it has in cyclones off Hawaii during eddy formation (Benitez-Nelson et al., 2007). As the sampling during the EDDIES cruises was limited to mature eddies, this type of ephemeral diatom bloom in forming cyclones may have been missed (Benitez-Nelson and McGillicuddy, 2008).

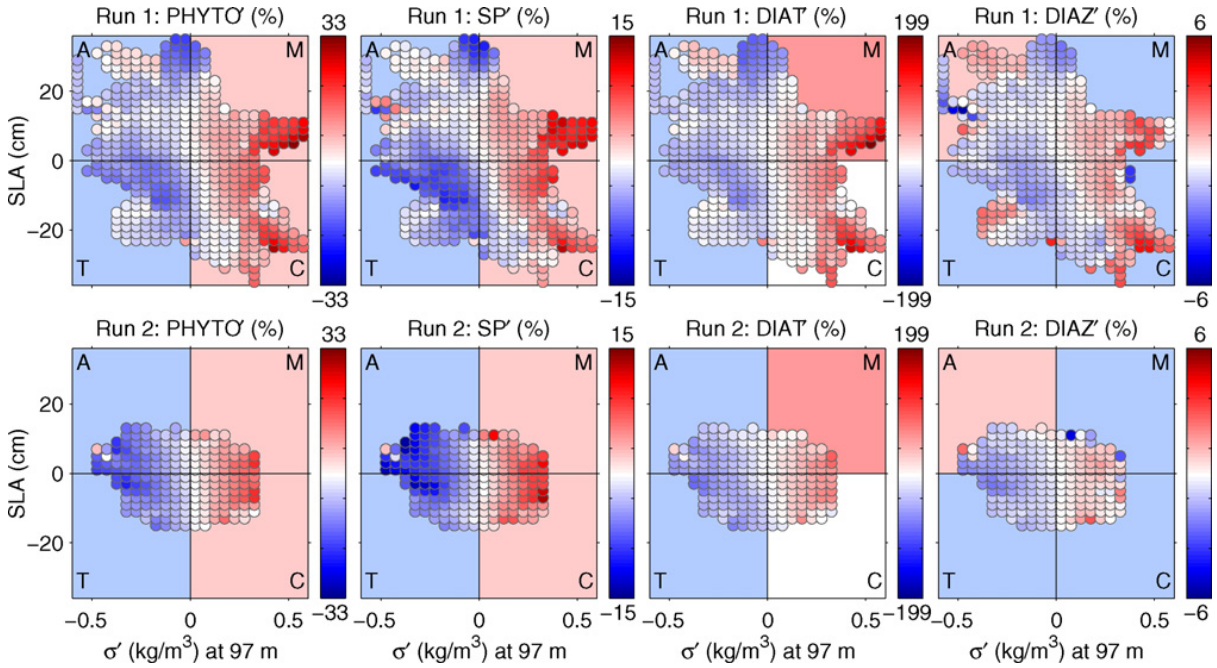

Fig. 8. Run 1 (no eddy/wind interaction, top row) and Run 2 (with eddy/wind interaction, bottom row) 0–104 m phytoplankton biomass anomalies (mg C m^{-2}), expressed as percent anomaly from the large-scale mean, binned according to SLA and in situ density anomaly at 97 m in the Sargasso Sea subdomain. The first column shows total phytoplankton biomass anomaly; second column, small phytoplankton biomass anomaly; third column, diatom biomass anomaly; fourth column, diazotroph biomass anomaly. The four quadrants correspond to anticyclones (A), mode-water eddies (M), thinnies (T) and cyclones (C). The background shading indicates the tendency of Sargasso Sea field data, e.g. diatom biomass anomalies are generally observed to be positive in mode-water eddies, negative in anticyclones and thinnies, with cyclones uncertain (see text, Section 4). Darker background shading of diatoms in mode-water eddies is used to reflect the fact that highest Chl anomalies have been observed in those features (Fig. 2A in McGillicuddy et al., 2007).

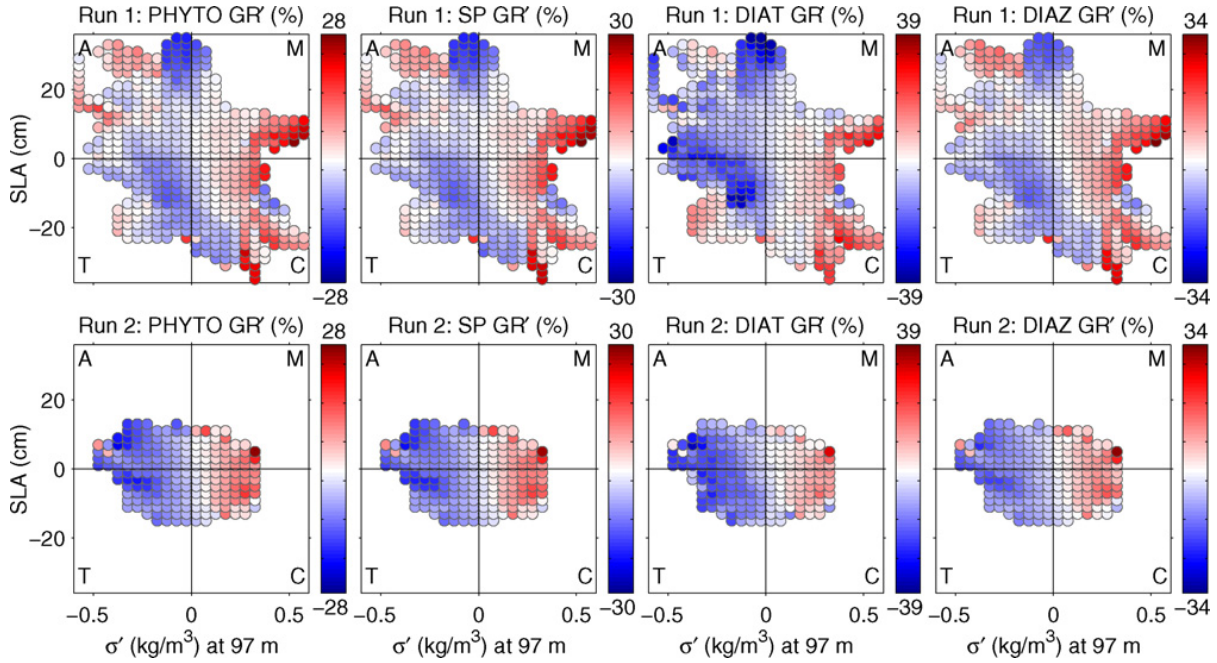

Fig. 9. Run 1 (no eddy/wind interaction, top row) and Run 2 (with eddy/wind interaction, bottom row) phytoplankton specific growth rate anomalies, binned according to in situ density anomaly and SLA, in the Sargasso Sea subdomain. The first column shows total phytoplankton specific growth rate (d^{-1}) anomalies, computed as 0–104 m primary production rates (mg C m^{-2} d^{-1}) divided by 0–104 m biomass (mg C m^{-2}), and expressed as percent anomaly from large-scale mean growth rates. The second column shows small phytoplankton growth rate anomalies; third column, diatom growth rate anomalies; fourth column, diazotroph growth rate anomalies. The four quadrants correspond to anticyclones (A), mode-water eddies (M), thinnies (T) and cyclones (C).

Accordingly, the background shading of the C quadrants in Fig. 8 has been left blank to reflect this uncertainty. Two EDDIES cyclones did show relatively low silicate concentrations at their centers, which may be indicative of prior diatom blooms (Li and Hansell, 2008). Alternatively Bibby and Moore (2010) have suggested the lack of diatom blooms in Sargasso Sea cyclones results from differences in silicate and nitrate concentrations of the upwelled water.

One clear discrepancy between simulated and observed species composition is that the model failed to reproduce the observed correlation of positive diazotroph biomass anomalies with anticyclones over cyclones. The reason may be related to any number of processes missing from the model. For example, *Trichodesmium* have gas vacuoles that allow them to be positively buoyant, potentially causing aggregation in regions of surface convergence. Such circumstances would be expected to occur during the genesis of anticyclones and throughout the lifetimes of thinnies and cyclones. The model diazotrophs, in contrast, currently have neutral buoyancy. Secondly, it has been recently discovered that *Trichodesmium* can utilize DOP (Dyhrman et al., 2006; Orchard et al., 2010). Preliminary simulations at 1.6° resolution show that this allows diazotrophs in the model to have highest biomass at the sea surface (in better agreement with observations), and should liberate their phosphorus-limited growth rates from association with cyclones and mode-water eddies. Thirdly, the temperature-dependence of their growth rate is actually much stronger than currently used in the model (Breitbarth et al., 2007). Finally, the enhancement of diazotrophs in anticyclones could reflect eddy-driven horizontal advection across a large-scale gradient. The simulated annual mean diazotroph meridional gradient between 22°N and 30°N along 60–68°W is only 5%, much smaller than the observed factor of two or more (Carpenter and Price, 1977; Carpenter and Romans, 1991). Therefore this possibility cannot be evaluated with the present model.

While the inclusion of eddy/wind interactions improved phytoplankton community structure (Figs. 6–9) and some aspects of eddy demographics (Fig. 4b), it degraded EKE (Fig. 1; cf. Scharffenberg and Stammer, 2010) and the magnitude of eddy SLA (Fig. 4c). An unrealistically weak eddy field potentially compromises both the physical and biological aspects of the simulation, so it is of interest to increase SLA variance back to observed levels. One possible way to increase EKE might be to decrease horizontal viscosity. The viscosity scheme we used was calibrated largely based on Gulf Stream separation (Plate 1 in Hecht et al., 2008); our Fig. 1 shows that the eddy/wind interaction does reduce spurious SLA variability to the southeast of Cape Hatteras, such that a further decrease in viscosity may be possible. However it is not clear if the viscosity can be decreased at this grid resolution without degrading other aspects of the physical simulation (Bryan et al., 2007), including increased numerical noise (Jochum et al., 2008) to which vertical velocities and consequently biological processes may be sensitive. If this does not prove successful, increased horizontal grid resolution probably will be required. While 0.1° resolution adequately resolves mesoscale eddies, it poorly resolves submesoscale processes that interact strongly with the mesoscale. Bryan et al. (2007) note that the 0.1° North Atlantic POP simulation's sensitivity to subgridscale parameterizations suggests the flow field is not yet at convergence. Hurlburt and Hogan (2000) found convergence of physical eddy statistics at approximately 0.03° resolution. We therefore anticipate a doubling or tripling of grid resolution would bring the eddy intensities back to the observed levels. This higher grid resolution should also improve the simulated nutrient fluxes and biological productivity associated with submesoscale processes at the edges of eddies, although even 0.03° resolution may not be sufficient for convergence of biological production (e.g., Lévy et al., 2001).

Similar to Eden and Dietze (2009), new production in the Sargasso subdomain decreased slightly (13%) from Run 1 to Run 2. However because the eddy intensities in Run 2 are lower than observed by roughly a factor of two, the eddy/wind interaction-driven vertical velocities are likely also underestimated by a factor of two. Consequently it is premature to assess the net impact of eddy/wind interaction on biological processes without first bringing the physical simulation into closer agreement with observations.

5. Conclusions

Including the eddy/wind interaction significantly changed the simulated physical properties of eddies in the Sargasso Sea, including the relative number of different types of eddies. This change in

model forcing gave closer agreement with observations regarding the total number of eddies, and the range of density anomalies at 97 m. The simulation with eddy/wind interaction also yielded similar isopycnal displacements and nitrate concentrations at the centers of mode-water eddies and cyclones. However EKE and SLA variance became lower than observed, and the proportion of thinnies to regular cyclones became higher than observed. Decreased horizontal viscosity or increased horizontal grid resolution appears necessary to restore the model EKE back toward observations, which is a prerequisite to assessing the full impact of eddy/wind interaction on physical and biological processes in the North Atlantic.

Including the eddy/wind interaction brings the biological simulation into closer phenomenological agreement with observed eddy–phytoplankton relationships, viz. significantly enhanced diatom biomass and growth rates in mode-water eddies, and slightly enhanced small phytoplankton biomass in mode-water eddies and cyclones. The simulation suggests in situ growth as being the primary cause of enhanced phytoplankton biomass found in cyclones and mode-water eddies, resulting from upward isopycnal displacements and elevated nutrients at the base of the euphotic zone. In contrast, the simulations did not reproduce enhanced diazotroph biomass in anticyclones, indicating that one or more processes are missing from the diazotroph parameterization.

Acknowledgements

We would like to thank Marjy Friedrichs for providing the Regional Testbed code, Jeff Dusenberry for implementation of the BEC model into the Regional Testbed, and Valery Kosnyrev for retrieval of the AVISO data. The simulations were run on the supercomputer Pleiades at NASA Ames Research Center using 512 parallel cores. LAA and DJM gratefully acknowledge the support of NASA grant 07-CARBON07-17. SCD and IDL gratefully acknowledge support from the NSF Center for Microbial Oceanography, Research and Education (C-MORE; NSF EF-0424599).

Appendix A. Supplementary data

Supplementary data associated with this article can be found, in the online version, at doi:10.1016/j.dynatmoce.2011.01.003.

References

Barnier, B., Siefridt, L., Marchesiello, P., 1995. Thermal forcing for a global ocean circulation model using a three-year climatology of ECMWF analyses. Journal of Marine Systems 6, 363–380.

Benitez-Nelson, C.R., Bidigare, R.R., Dickey, T.D., Landry, M.R., Leonard, C.L., Brown, S.L., Nencioli, F., Rii, Y.M., Maiti, K., Becker, J.W., Bibby, T.S., Black, W., Cai, W.J., Carlson, C.A., Chen, F.Z., Kuwahara, V.S., Mahaffey, C., McAndrew, P.M., Quay, P.D., Rappe, M.S., Selph, K.E., Simmons, M.P., Yang, E.J., 2007. Mesoscale eddies drive increased silica export in the subtropical Pacific Ocean. Science 316 (5827), 1017–1021.

Benitez-Nelson, C.R., McGillicuddy, D.J., 2008. Mesoscale physical–biological–biogeochemical linkages in the open ocean: an introduction to the results of the E-FLUX and EDDIES programs. Deep-Sea Research II 55 (10–13), 1133–1138.

Bibby, T.S., Moore, C.M., 2010. Silicate:nitrate ratios of upwelled waters control the phytoplankton community sustained by mesoscale eddies in sub-tropical North Atlantic and Pacific. Biogeosciences Discussions 7, 7505–7525.

Boyer, T.P., Stephens, C., Antonov, J.I., Conkright, M.E., Locarnini, R.A., O'Brien, T.D., Garcia, H.E., 2002. World Ocean Atlas 2001, vol. 2. Salinity. In: Levitus, S. (Ed.), NOAA Atlas NESDIS 50. U.S. Government Printing Office, Washington, DC, 165 pp.

Brachet, S.P., Le Traon, P.Y., Le Provost, C., 2004. Mesoscale variability from a high-resolution model and from altimeter data in the North Atlantic Ocean. Journal of Geophysical Research – Oceans 109C, C12025.

Breitbarth, E., Oschlies, A., LaRoche, J., 2007. Physiological constraints on the global distribution of *Trichodesmium*—effect of temperature on diazotrophy. Biogeosciences 4, 53–61.

Bryan, F.O., Hecht, M.W., Smith, R.D., 2007. Resolution convergence and sensitivity studies with North Atlantic circulation models. Part I. The western boundary current system. Ocean Modelling 16, 141–159.

Carpenter, E.J., Price, C.C., 1977. Nitrogen fixation, distribution, and production of *Oscillatoria* (*Trichodesmium*) spp. in the western Sargasso and Caribbean Seas. Limnology and Oceanography 22, 60–72.

Carpenter, E.J., Romans, K., 1991. Major role of the cyanobacterium *Trichodesmium* in nutrient cycling in the North Atlantic Ocean. Science 254, 1356–1358.

Conkright, M.E., Garcia, H.E., O'Brien, T.D., Locarnini, R.A., Boyer, T.P., Stephens, C., Antonov, J.I., 2002. World Ocean Atlas 2001, vol. 4. Nutrients. In: Levitus, S. (Ed.), NOAA Atlas NESDIS 52. U.S. Government Printing Office, Washington, DC, 392 pp.

Davis, C.S., McGillicuddy, D.J., 2006. Transatlantic abundance of the N_2-fixing colonial cyanobacterium *Trichodesmium*. Science 312, 1517–1520.

Dewar, W.K., Flierl, G.R., 1987. Some effects of wind on rings. Journal of Physical Oceanography 17, 1653–1667.

Ducklow, H.W., Harris, R.P., 1993. Introduction to the JGOFS North Atlantic Bloom Experiment. Deep-Sea Reasearch II 40 (1–2), 1–8.
Dyhrman, S.T., Chappell, P.D., Haley, S.T., Moffett, J.W., Orchard, E.D., Waterbury, J.B., Webb, E.A., 2006. Phosphonate utilization by the globally important marine diazotroph *Trichodesmium*. Nature 439 (7072), 68–71.
Eden, C., Dietze, H., 2009. Effects of mesoscale eddy/wind interactions on biological new production and eddy kinetic energy. Journal of Geophysical Research – Oceans 114 (C5), C05023.
Ewart, C.S., Meyers, M.K., Wallner, E.R., McGillicuddy, D.J., Carlson, C.A., 2008. Microbial dynamics in cyclonic and anticyclonic mode-water eddies in the northwestern Sargasso Sea. Deep-Sea Research II 55 (10–13), 1334–1347.
Friedrichs, M.A.M., Dusenberry, J.A., Anderson, L.A., Armstrong, R.A., Chai, F., Christian, J.R., Doney, S.C., Dunne, J., Fujii, M., Hood, R., McGillicuddy, D.J., Moore, J.K., Schartau, M., Spitz, Y.H., Wiggert, J.D., 2007. Assessment of skill and portability in regional marine biogeochemical models: role of multiple planktonic groups. Journal of Geophysical Research – Oceans 112 (C8), C08001.
Garcia, H.E., Locarnini, R.A., Boyer, T.P., Antonov, J.I., 2006a. World Ocean Atlas 2005, vol. 3. Dissolved oxygen, apparent oxygen utilization, and oxygen saturation. In: Levitus, S. (Ed.), NOAA Atlas NESDIS 63. U.S. Government Printing Office, Washington, DC, 342 pp.
Garcia, H.E., Locarnini, R.A., Boyer, T.P., Antonov, J.I., 2006b. World Ocean Atlas 2005, vol. 4. Nutrients (phosphate, nitrate, silicate). In: Levitus (Ed.), NOAA Atlas NESDIS 64. U.S. Government Printing Office, Washington, DC, 396 pp.
Hecht, M.W., Petersen, M.R., Wingate, B.A., Hunke, E., Maltrud, M., 2008. Lateral mixing in the eddying regime and a new broad-ranging formulation. In: Hecht, M.W., Hasumi, H. (Eds.), Ocean Modeling in an Eddying Regime, Geophysical Monograph Series 177. American Geophysical Union, Washington, DC, pp. 339–352.
Hurlburt, H.E., Hogan, P.J., 2000. Impact of 1/8° to 1/64° resolution on Gulf Stream model-data comparisons in basin-scale subtropical Atlantic Ocean models. Dynamics of Atmospheres and Oceans 32, 283–329.
Jochum, M., Danabasoglu, G., Holland, M., Kwon, Y.-O., Large, W.G., 2008. Ocean viscosity and climate. Journal of Geophysical Research – Oceans 113C, C06017.
Key, R.M., Kozyr, A., Sabine, C.L., Lee, K., Wanninkhof, R., Bullister, J.L., Feeley, R.A., Millero, F.J., Mordy, C., Peng, T.-H., 2004. A global ocean carbon climatology: results from Global Data Analysis Project (GLODAP). Global Biogeochemical Cycles 18, GB4031.
Krause, J.W., Nelson, D.M., Lomas, M.W., 2010. Production, dissolution, accumulation, and potential export of biogenic silica in a Sargasso Sea mode-water eddy. Limnology and Oceanography 55, 569–579.
Large, W.G., McWilliams, J.C., Doney, S.C., 1994. Oceanic vertical mixing: a review and a model with a nonlocal boundary layer parameterization. Reviews of Geophysics 32, 363–403.
Large, W.G., Pond, S., 1981. Open ocean momentum flux measurements in moderate to strong winds. Journal of Physical Oceanography 11, 324–336.
Large, W.G., Pond, S., 1982. Sensible and latent heat flux measurements over the ocean. Journal of Physical Oceanography 12, 464–482.
Large, W.G., Yeager, S.G., 2004. Diurnal to decadal global forcing for ocean and sea-ice models: the data sets and flux climatologies. In: NCAR Technical Note NCAR/TN-460 + STR, Climate and Global Dynamics Division. National Center for Atmospheric Research, Boulder, CO.
Ledwell, J.R., McGillicuddy, D.J., Anderson, L.A., 2008. Nutrient flux into an intense deep chlorophyll layer in a mode-water eddy. Deep-Sea Research II 55 (10–13), 1139–1160.
Lévy, M., Klein, P., Treguier, A.-M., 2001. Impact of sub-mesoscale physics on production and subduction of phytoplankton in an oligotrophic regime. Journal of Marine Research 59 (4), 535–565.
Li, Q.P., Hansell, D.A., 2008. Nutrient distributions in baroclinic eddies of the oligotrophic North Atlantic and inferred impacts on biology. Deep-Sea Research II 55 (10–13), 1291–1299.
Locarnini, R.A., O'Brien, T.D., Garcia, H.E., Antonov, J.I., Boyer, T.P., Conkright, M.E., Stephens, C., 2002. World Ocean Atlas 2001, vol. 3. Oxygen. In: Levitus, S. (Ed.), NOAA Atlas NESDIS 51. U.S. Government Printing Office, Washington, DC, 286 pp.
Martin, A.P., Richards, K.J., 2001. Mechanisms for vertical nutrient transport within a North Atlantic mesoscale eddy. Deep-Sea Research II 48, 757–773.
McClean, J.L., Poulain, P.-M., Pelton, J.W., Maltrud, M.E., 2002. Eulerian and Lagrangian statistics from surface drifters and a high-resolution POP simulation in the North Atlantic. Journal of Physical Oceanography 32, 2472–2491.
McGillicuddy, D.J., Anderson, L.A., Doney, S.C., Maltrud, M.E., 2003. Eddy-driven sources and sinks of nutrients in the upper ocean: results from a 0.1 degree resolution model of the North Atlantic. Global Biogeochemical Cycles 17 (2), 1035, doi:10.1029/2002GB001987.
McGillicuddy, D.J., Anderson, L.A., Bates, N.R., Bibby, T., Buesseler, K.O., Carlson, C.A., Davis, C.S., Ewart, C., Falkowski, P.G., Goldthwait, S.A., Hansell, D.A., Jenkins, W.J., Johnson, R., Kosnyrev, V.K., Ledwell, J.R., Li, Q.P., Siegel, D.A.S., Steinberg, D.K., 2007. Eddy/wind interactions stimulate extraordinary mid-ocean plankton blooms. Science 316, 1021–1026.
McGillicuddy, D.J., Johnson, R., Siegel, D.A., Michaels, A.F., Bates, N.R., Knap, A.H., 1999. Mesoscale variations of biogeochemical properties in the Sargasso Sea. Journal of Geophysical Research – Oceans 104 (C6), 13,381–13,394.
Moore, J.K., Doney, S.C., Lindsay, K., 2004. Upper ocean ecosystem dynamics and iron cycling in a global three-dimensional model. Global Biogeochemical Cycles 18, GB4028.
Moore, J.K., Doney, S.C., Lindsay, K., Mahowald, N., Michaels, A.F., 2006. Nitrogen fixation amplifies the ocean biogeochemical response to decadal timescale variations in mineral dust deposition. Tellus 58B, 560–572.
Moore, J.K., Doney, S.C., 2007. Iron availability limits the ocean nitrogen inventory stabilizing feedbacks between marine denitrification and nitrogen fixation. Global Biogeochemical Cycles 21 (2), GB2001.
Mouriño-Carballido, B., 2009. Eddy-driven pulses of respiration in the Sargasso Sea. Deep-Sea Research I 56 (8), 1242–1250.
Orchard, E.D., Ammerman, J.W., Lomas, M.W., Dyhrman, S.T., 2010. Dissolved inorganic and organic phosphorus uptake in *Trichodesmium* and the microbial community: the importance of phosphorus ester in the Sargasso Sea. Limnology and Oceanography 55, 1390–1399.
Oschlies, A., Garcon, V., 1999. An eddy-permitting coupled physical–biological model of the North Atlantic. 1. Sensitivity to physics and numerics. Global Biogeochemical Cycles 13, 135–160.

Pacanowski, R.C., Philander, S.G.H., 1981. Parameterization of vertical mixing in numerical models of the tropical oceans. Journal of Physical Oceanography 11, 1443–1451.
Scharffenberg, M.G., Stammer, D., 2010. Seasonal variations of the large-scale geostrophic flow field and eddy kinetic energy inferred from the TOPEX/Poseidon and Jason-1 tandem mission data. Journal of Geophysical Research – Oceans 115 (C), C02008.
Small, R.J., Richards, K.J., Xie, S.-P., Dutrieux, P., Miyama, T., 2009. Damping of tropical instability waves caused by the action of surface currents on stress. Journal of Geophysical Research – Oceans 114, C04009.
Smith, R.D., Dukowicz, J.K., Malone, R.C., 1992. Parallel ocean circulation modeling. Physica D 60, 38–61.
Smith, R., Maltrud, M., Bryan, F., Hecht, M., 2000. Numerical simulation of the North Atlantic Ocean at 1/10°. Journal of Physical Oceanography 30, 1532–1561.
Stammer, D., Wunsch, C., Ueyoshi, K., 2006. Temporal changes in ocean eddy transports. Journal of Physical Oceanography 36, 543–550.
Steinberg, D.K., Carlson, C.A., Bates, N.R., Johnson, R.J., Michaels, A.F., Knap, A.H., 2001. Overview of the US JGOFS Bermuda Atlantic Time-series Study (BATS): a decade-scale look at ocean biology and biogeochemistry. Deep-Sea Research II 48 (8–9), 1405–1447.
Stephens, C., Antonov, J.I., Boyer, T.P., Conkright, M.E., Locarnini, R.A., O'Brien, T.D., Garcia, H.E., 2002. World Ocean Atlas 2001, vol. 1. Temperature. In: Levitus, S. (Ed.), NOAA Atlas NESDIS 49. U.S. Government Printing Office, Washington, DC, 167 pp.
Sweeney, E.N., McGillicuddy, D.J., Buesseler, K.O., 2003. Biogeochemical impacts due to mesoscale eddy activity in the Sargasso Sea as measured at the Bermuda Atlantic Time Series (BATS) site. Deep-Sea Research II 50, 3017–3039.
Tokmakian, R., McClean, J.L., 2003. How realistic is the high frequency signal of a 0.1° resolution ocean model? Journal of Geophysical Reasearch – Oceans 108 (C4), 3115.
Xu, Y., Scott, R.B., 2008. Subtleties in forcing eddy resolving ocean models with satellite wind data. Ocean Modelling 20 (3), 240–251.
Zhai, X., Greatbatch, R.J., 2007. Wind work in a model of the northwest Atlantic Ocean. Geophysical Research Letters 34, L04606.